International Journal of Thermophysics, Vol. 27, No. 5, September 2006 (© 2006)
DOI: 10.1007/s10765-006-0111-9

An Extended Equation of State Modeling Method I. Pure Fluids

G. Scalabrin,[1] L. Bettio,[1] P. Marchi,[1] L. Piazza,[2] and D. Richon[3,4]

Received January 30, 2006

A new technique is proposed here to represent the thermodynamic surface of a pure fluid in the fundamental Helmholtz energy form. The peculiarity of the present method is the extension of a generic equation of state for the target fluid, which is assumed as the basic equation, through the distortion of its independent variables by individual shape functions, which are represented by a neural network used as function approximator. The basic equation of state for the target fluid can have the simple functional form of a cubic equation, as, for instance, the Soave–Redlich–Kwong equation assumed in the present study. A set of nine fluids including hydrocarbons, haloalkane refrigerants, and strongly polar substances has been considered. For each of them the model has been regressed and then validated against volumetric and caloric properties generated in the vapor, liquid, and supercritical regions from highly accurate dedicated equations of state. In comparison with the underlying cubic equation of state, the prediction accuracy is improved by a factor between 10 and 100, depending on the property and on the region. It has been verified that about 100 density experimental points, together with from 10 to 20 coexistence data, are sufficient to guarantee high prediction accuracy for different thermodynamic properties. The method is a promising modeling technique for the heuristic development of multiparameter dedicated equations of state from experimental data.

KEY WORDS: cubic equation of state; extended equation of state; feed forward neural network; fundamental equation of state; Helmholtz energy equation; pure fluids; thermodynamic properties.

[1] Dipartimento di Fisica Tecnica, Università di Padova, via Venezia 1, I-35131 Padova, Italy.
[2] Thermodynamics and Energy Technologies (ThEt), University of Paderborn, D-33095 Paderborn, Germany.
[3] Centre Energétique et Procédés, Ecole Nationale Supérieure des Mines de Paris CEP/TEP, 35 rue Saint Honoré, 77305 Fontainebleau, France.
[4] To whom correspondence should be addressed. E-mail: dominique.richon@ensmp.fr

1. INTRODUCTION

The representation of thermodynamic properties of a pure fluid with the highest accuracy is one of the main tasks of thermodynamic modeling. Fundamental multiparameter equations of state (EoS) were developed allowing any thermodynamic function to be calculated by simple mathematical differentiation. The EoSs pertaining to this category can be regressed only where the thermodynamic behavior of the target fluid is well known from a wide number of precise experimental data. The obtained dedicated equations of state (DEoS) are specific for each fluid of interest. The accuracies of their predictions are at the same level as the experimental uncertainty of the available measurements.

The established procedure to develop wide-range fundamental EoSs, due to the pioneering activity of Wagner and co-workers [1–3], is heuristic and non-theoretically founded because the EoS functional form is shaped and optimized directly on the database through powerful optimization methods.

In recent times, the extended corresponding states (ECS) modeling technique [4–9] was also extensively studied to verify whether it could be improved to obtain a further method for the development of wide-range fundamental EoSs. A new heuristic procedure descending from the conventional ECS technique was recently proposed for the haloalkanes in a predictive mode [10] and in a correlative mode [11]; moreover, a wide-range fundamental EoS dedicated to fluoropropane (R227ea) was obtained [12].

In the present work, the ECS framework is exploited to turn this technique into a further flexible heuristic method for the development of a highly accurate fundamental EoS dedicated to a target fluid. The search for a convenient reference fluid fulfilling a "conformality condition" with the target fluid, as required by the ECS methods, is avoided here because the EoS for the reference fluid is substituted by an equation for the target fluid itself. Such an equation is improved and extended through the application of the proposed modeling technique.

2. FUNDAMENTAL EQUATIONS OF STATE

An equation of state for a pure fluid can be expressed in terms of the molar Helmholtz free energy A as a function of the independent variables temperature T and density ρ. The dimensionless Helmholtz energy $a = A/(RT)$ is split into two contributions, i.e., the ideal part a° and the residual part a^R:

$$a(T,\rho)=\frac{A}{RT}=\frac{A^\circ}{RT}+\frac{A^R}{RT}=a^\circ(T,\rho)+a^R(T,\rho), \tag{1}$$

where R is the molar gas constant. The definition of the Helmholtz energy for a fluid in the ideal-gas state A° is

$$A^\circ(T,\rho)=U^\circ(T)-TS^\circ(T,\rho)=H^\circ(T)-RT-TS^\circ(T,\rho), \tag{2}$$

where the internal energy U°, enthalpy H°, and entropy S° of the ideal gas can be calculated from an equation for the ideal-gas isobaric heat capacity C_p°. Consequently the dimensionless ideal part a° reads

$$a^\circ(T,\rho)=\frac{A^\circ(T,\rho)}{RT}=\frac{H_o^\circ}{RT}-\frac{S_o^\circ}{R}-1+\frac{1}{RT}\int_{T_o}^{T}C_p^\circ(T)\mathrm{d}T -\frac{1}{R}\int_{T_o}^{T}\frac{C_p^\circ(T)}{T}\mathrm{d}T+\ln\left(\frac{T\rho}{T_o\rho_o}\right), \tag{3}$$

where H_o° and S_o° are the enthalpy and entropy values of the ideal gas at a reference state (T_o, ρ_o). Therefore, the individual $C_p^\circ(T)$ function for the fluid of interest is the only element required for calculation of the ideal part a°.

The Helmholtz energy equation of a fluid in the temperature and density variables is a fundamental equation of state, i.e., any thermodynamic property can be obtained from it through a suitable combination of derivatives of its form and no integral calculation is required [1, 3]. In general, apart from a few cases such as the speed of sound, any thermodynamic quantity m can be represented as

$$m(T,\rho)=m^\circ(T,\rho)+m^R(T,\rho). \tag{4}$$

The ideal part m°, which for some properties is a function of T only, can be obtained either through differentiation of the ideal part a° of the fundamental equation of state or directly from the basic definition of the quantity m° in which the $C_p^\circ(T)$ function and its mathematical transformations are present. In both cases the required input is limited to the individual function $C_p^\circ(T)$. The residual part m^R is calculated from the residual part a^R through a combination of derivatives of its functional form according to classical thermodynamics [1, 3].

The basic target of the development of an equation of state is then to provide an equation for the residual part a^R, from which all the properties are obtained. This is the aim also of the modeling technique proposed herein.

3. ECS BASIC MODELING

A rigorous derivation of the corresponding-states principle is given by statistical mechanics [13, 14] under the hypothesis of similarity between the molecular potentials of different fluids. Fluids satisfying such a hypothesis are said to be *conformal*.

For conformal fluids the similarity of their reduced residual Helmholtz free energies can be demonstrated [15, 16] and it is expressed as

$$a_j^{\mathrm{R}}(T_j, \rho_j) = a_0^{\mathrm{R}}(T_0, \rho_0) = a_0^{\mathrm{R}}(T_j/f_j, \rho_j h_j), \tag{5}$$

where the subscripts 0 and j denote the reference and the target fluid, respectively. In case of perfectly conformal fluids the *scale factors* f_j and h_j simply coincide with the ratios of the critical constants:

$$f_j = T_{\mathrm{c},j}/T_{\mathrm{c},0} \tag{6}$$

$$h_j = \rho_{\mathrm{c},0}/\rho_{\mathrm{c},j}. \tag{7}$$

Since the conformality condition is exactly attained only for a very limited number of fluids, it is convenient to introduce two empirical correction factors, which are called *shape functions* and are denoted as θ_j and ϕ_j:

$$f_j = \frac{T_{\mathrm{c},j}}{T_{\mathrm{c},0}}\theta_j(T_j, \rho_j) \tag{8}$$

$$h_j = \frac{\rho_{\mathrm{c},0}}{\rho_{\mathrm{c},j}}\phi_j(T_j, \rho_j). \tag{9}$$

The differentiation of Eq. (5) with respect to T_j and ρ_j gives the following equations, respectively:

$$\left(\frac{\partial a_j^{\mathrm{R}}}{\partial T_j}\right)_{\rho_j} = -\frac{u_j^{\mathrm{R}}}{T_j} = -\frac{u_0^{\mathrm{R}}(1-F_T) - Z_0^{\mathrm{R}} H_T}{T_j} \tag{10}$$

$$\left(\frac{\partial a_j^{\mathrm{R}}}{\partial \rho_j}\right)_{T_j} = \frac{Z_j^{\mathrm{R}}}{\rho_j} = \frac{u_0^{\mathrm{R}} F_\rho + Z_0^{\mathrm{R}}(1+H_\rho)}{\rho_j}. \tag{11}$$

In the former two equations, the four logarithmic derivatives of the scale factors F_T, F_ρ, H_T, and H_ρ are defined as

$$F_T = \frac{T_j}{f_j}\left(\frac{\partial f_j}{\partial T_j}\right)_{\rho_j} \tag{12}$$

$$F_\rho = \frac{\rho_j}{f_j}\left(\frac{\partial f_j}{\partial \rho_j}\right)_{T_j} \tag{13}$$

$$H_T = \frac{T_j}{h_j}\left(\frac{\partial h_j}{\partial T_j}\right)_{\rho_j} \tag{14}$$

$$H_\rho = \frac{\rho_j}{h_j}\left(\frac{\partial h_j}{\partial \rho_j}\right)_{T_j} \tag{15}$$

Equations (10) and (11) allow for calculation of the residual compressibility factor $Z_j^{\mathrm{R}} = Z_j - 1$ and of the reduced residual internal energy $u_j^{\mathrm{R}} = U_j^{\mathrm{R}}/(RT_j)$ of the target fluid, once an EoS for the reference fluid and the equations for the scale factors are available. Analogous formulations are obtained for any other thermodynamic function of the target fluid, and greater details are given in Refs. 4 and 11. A summary of the equations required for the property calculations is given in the Appendix.

The ECS model was extensively developed from the late 1970s until the early 1990s as a mean for the prediction and correlation of thermophysical properties for pure fluids and mixtures [4, 5]. In these traditional approaches, the determination of the scale factors as continuous functions of temperature and density was never attained. In some studies the scale factors, and then the shape functions, were locally calculated from the solution of an equation system composed of Eq. (5) plus a supplementary condition. The solution of such a system is possible only if DEoSs for both fluids are available [4].

Lately, the ECS method was revisited by some authors [8–12, 17], who independently determined the shape functions through a minimization procedure using experimental data of various properties for the fluid of interest, making the method similar to the classical multiproperty fitting approach [1–3]. In such a way both the shape functions become available as continuous analytical functions of temperature and density.

In particular, in the works of Scalabrin et al. [10–12, 17] an artificial neural network (ANN) was assumed as a general function approximator for the representation of the shape functions. This work was focused on the refrigerant family both as pure fluids [11] and as mixtures [17], always assuming R134a as the reference fluid.

In any case, the fundamental condition for the applicability of an ECS technique is a basic conformality between the target and the reference fluid or, extensively, among all the target fluids pertaining to the same family of the reference fluid.

4. EXTENDED EQUATION OF STATE MODEL: MATHEMATICAL FORMULATION

In case that either the conformality condition does not hold for the fluids of a family or a precise DEoS is not available for any component of the family, whose fluids are supposed to share a conformality condition, the ECS methods cannot be reliably applied. In fact, the purpose of such methods is to obtain a DEoS for the target fluid through the correction of the DEoS of the reference fluid, assumed to be conformal with the target fluid, by the distortion of its independent variables with suitable shape functions. Where the corresponding states conformality fails, the similarity connection among the fluids of the family is no longer sustainable and the method becomes ineffective. On the other hand, the unavailability of a reference DEoS practically prevents the application of the method, with an equivalent final result of failure of the modeling technique.

The present proposal aims at overcoming such a limitation performing the correction by the variables distortion of a simple EoS, which roughly represents the target fluid itself, instead of the DEoS of a reference fluid, avoiding in this way any problem about the fulfillment of the conformality condition. In fact, it would no longer be necessary to have a "reference fluid," following the classical interpretation of the ECS theory, but only a "reference equation" for the target fluid itself, whose precision is enhanced, or "extended," through the application of the shape functions. Hence, the name of *extended equation of state* (EEoS) has been chosen to denote this new modeling method. Anyway, to avoid any misunderstanding, in the following the term "reference equation" is substituted with "basic equation."

As a consequence of this new procedure, in Eqs. (8) and (9) the $T_{c,j}$ and $\rho_{c,j}$ critical parameters coincide with $T_{c,0}$ and $\rho_{c,0}$, respectively, since the target fluid and the reference fluid are the same. In the present case it follows that

$$f_j = \theta_j(T_j, \rho_j) \qquad h_j = \phi_j(T_j, \rho_j) \tag{16,17}$$

The simplest, but at the same time sound, EoS that can be chosen for the present purpose is a cubic EoS in one of its more recurrent versions. In fact it has general applicability to practically any fluid because it requires only critical data and a few vapor pressure values to calculate the individual acentric factor. Anyway, the proposed method is not restricted to the choice of a cubic EoS but any EoS, represented in the fundamental Helmholtz energy form, can be suitably considered, provided that the independent variables to which the shape functions distortion is applied are T and ρ. If, for instance, a DEoS for the target fluid has to be updated after

the publication of new data sets, this equation can be directly considered as the basic EoS from which to develop a new and updated DEoS.

As will be shown later, the shape functions $\theta(T, \rho)$ and $\phi(T, \rho)$ are to be regressed forcing the model to represent known values of experimentally accessible thermodynamic quantities. Their functional formulation is here heuristically obtained applying a multi-layer feedforward neural network (MLFN) as a universal function approximator. Since the proposed modeling technique comes from the combination of the EEoS method with neural networks (NN), it is concisely indicated from now on as EEoS–NN model.

4.1. Cubic Basic EoS

The EEoS model is here developed assuming a cubic EoS as the reference for the target fluid in order to assure a broad applicability of the present model. Among the cubic EoSs, the Soave–Redlich–Kwong (SRK) equation [18, 19] was chosen. Mollerup [20] already proposed to determine the shape functions of a fluid with respect to a reference fluid representing both fluids through a SRK cubic EoS. This approach is only partially adopted here, because in the present work the reference fluid coincides with the fluid of interest, so the basic EoS is represented by the SRK equation for the fluid itself. Moreover, the shape factors are here determined directly with experimental data using an advanced heuristic technique.

The SRK cubic EoS in the temperature T and molar volume v variables is expressed as

$$P = \frac{RT}{v-b} - \frac{a_{\mathrm{SRK}}}{(v+b)v} \tag{18}$$

with

$$a_{\mathrm{SRK}} = 0.42748 \frac{(RT_{\mathrm{c}})^2}{P_{\mathrm{c}}} \alpha(T_{\mathrm{r}}) \tag{19}$$

$$b = 0.08664 \frac{RT_{\mathrm{c}}}{P_{\mathrm{c}}} \tag{20}$$

The parameter a_{SRK} incorporates the function $\alpha(T_{\mathrm{r}})$ dependent on the reduced temperature $T_{\mathrm{r}} = T/T_{\mathrm{c}}$:

$$\alpha(T_{\mathrm{r}}) = \left\{1 + k(\omega)\left[1 - \sqrt{T_{\mathrm{r}}}\right]\right\}^2, \tag{21}$$

where k depends on the acentric factor ω, also known as Pitzer's parameter, according to

$$k(\omega) = c_1 + c_2\omega + c_3\omega^2 \tag{22}$$

with $c_1 = 0.480$, $c_2 = 1.574$, and $c_3 = -0.176$.

The SRK equation, as any cubic equation, gives only "reasonable" trends of the thermodynamic quantities rather than precise values. For example, it cannot represent the density with a sufficient accuracy; deviations in density may exceed 10% in vapor, liquid, and supercritical regions [21]. These shortcomings are due to the elementary mathematical form and to the low number of adjustable parameters. A simple but effective modification was proposed by Peneloux et al. [22] with the introduction of the *volume translation* to improve the representation of the liquid-phase density; the volume v is *shifted* by a constant c, which is determined with saturated-liquid-density data. The SRK EoS with volume translation, which is the form assumed here, reads

$$P = \frac{RT}{v + c - b} - \frac{a_{\mathrm{SRK}}}{(v + c + b)(v + c)} \tag{23}$$

In the present work the fluid-specific coefficient c was determined on a saturated-liquid density value generated from the DEoS for the target fluid at $T_r = 0.7$. For the considered fluids the critical constants, the parameters ω and c, together with the references for the DEoSs from which the saturated liquid densities were calculated, are listed in Table I.

A basic requirement of the present modeling technique is to obtain a DEoS in the fundamental form $a(T, \rho)$, which allows the calculation of any thermodynamic quantity only by combining derivatives. Therefore,

Table I. Critical Constants and Parameters for the Considered Pure Fluids

Fluid	T_c (K)	P_c (MPa)	ω	c ($\mathrm{L \cdot mol^{-1}}$)	Reference (DEoS)
C_2H_6	305.33	4.8718	0.0993	2.86496×10^{-3}	[23]
C_3H_8	369.85	4.24766	0.15242	5.20115×10^{-3}	[24]
n-C_4H_{10}	425.16	3.796	0.19959	7.85903×10^{-3}	[24]
R32	351.255	5.782	0.2768	1.29133×10^{-2}	[25]
R125	339.33	3.629	0.30349	7.79698×10^{-3}	[26]
R134a	374.18	4.05629	0.32689	1.13412×10^{-2}	[27]
R143a	346.04	3.7756	0.26113	1.34996×10^{-2}	[28]
NH_3	405.4	11.333	0.25601	7.23145×10^{-3}	[29]
H_2O	647.096	22.064	0.344	7.59369×10^{-3}	[30]

the SRK EoS is transformed into the Helmholtz energy form using the relation:

$$a^{\mathrm{R}} = \frac{1}{RT}\int_{v=\infty}^{v}\left(\frac{RT}{v} - P\right)\Big|_{T=\mathrm{const}} \mathrm{d}v, \tag{24}$$

where Eq. (23) is used to calculate P. This approach results in

$$a^{\mathrm{R}} = \ln\left(\frac{v}{v+c-b}\right) - \frac{a_{\mathrm{SRK}}}{RTb}\ln\left(\frac{v+c+b}{v+c}\right) \tag{25}$$

It is convenient to rewrite this equation as a function of density, remembering that $v = 1/\rho$. The Helmholtz energy basic equation, denoted with the subscript 0, finally reads

$$a_0^{\mathrm{R}} = -\ln[1+(c-b)\rho_0] - \frac{a_{\mathrm{SRK}}}{RT_0 b}\ln\left[\frac{1+(c+b)\rho_0}{1+c\rho_0}\right]. \tag{26}$$

The thermodynamic surface represented by such a basic equation is modified distorting its independent variables T and ρ by the shape functions θ_j and ϕ_j as empirical correction functions.

The thermodynamic properties obtained from differentiation of Eq. (26) represent the quantities of the basic equation which, indicated with subscript 0, enter into Eqs. (5), (10), (11), and the other ones that can be written for further properties.

4.2. Multi-Layer Feedforward Neural Networks

The determination of the residual Helmholtz energy $a_j^{\mathrm{R}}(T_j, \rho_j)$ for the target fluid is possible only after the shape functions have been determined. This subsequently allows any other residual function to be calculated through the first and second derivatives of $a_j^{\mathrm{R}}(T_j, \rho_j)$ with respect to temperature and density. In the present work the shape functions are expressed in the form of a multi-layer feedforward neural network. The general architecture of MLFN is illustrated in Fig. 1; it consists of three layers, respectively called *input*, *hidden*, and *output* layer.

The neurons of the input layer are indicated as elements of an array U of dimension I. Their number coincides with the number of independent variables of the system, in this case, the temperature and density of the fluid, plus one. The last neuron, labeled Bias1, is a constant with a convenient value assigned to it:

$$U_I = \mathrm{Bias1} \tag{27}$$

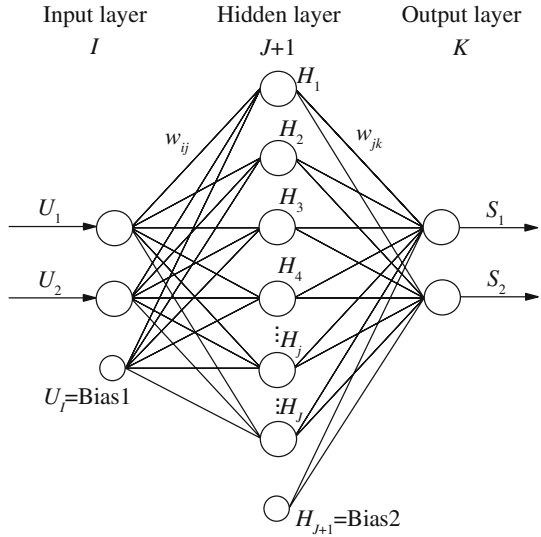

Fig. 1. General topology of a three-layer feedforward neural network with two output functions.

In the output layer the number of neurons equals the output quantities, which in this case are the two shape functions $\theta_j(T_j, \rho_j)$ and $\phi_j(T_j, \rho_j)$. They are indicated as elements of an array S of dimension K. Therefore, for the present problem the dimensions of the input and output layers are, respectively, $I = 3$ and $K = 2$.

The hidden layer, which performs the transformation of the signals from the input layer to the output layer, contains an arbitrary number of neurons. They are indicated as elements of a vector H of dimension $J+1$. The more neurons are used, the better is the approximation capability of the MLFN. Conversely, as the number of free parameters grows, the computation time rises and the problem of overfitting becomes relevant; a compromise is then required. In the hidden layer there is also a bias neuron, Bias2, just like in the input layer:

$$H_{J+1} = \text{Bias2} \tag{28}$$

Both the Bias1 and Bias2 values have been set to 1.

The input signals undergo a linear transformation to normalize them in the arbitrarily chosen range $[A_{\min}, A_{\max}]$ set at $A_{\min} = 0.05$ and $A_{\max} = 0.95$. The normalization is done according to

$$U_i = u_i(V_i - V_{i,\min}) + A_{\min} \quad 1 \le i \le I - 1 \tag{29}$$

with

$$u_i = \frac{A_{\max} - A_{\min}}{V_{i,\max} - V_{i,\min}} \tag{30}$$

Here $V_{i,\min}$ and $V_{i,\max}$ represent the lower and upper limits of the independent variable V_i, i.e., of temperature and density:

$$V_1 = T_j \tag{31}$$

$$V_2 = \rho_j \tag{32}$$

These limits represent also the validity limits of the obtained equation of state, because the extrapolation of temperature and density outside such ranges may result in unreliable calculated values. A transfer function g in the form of an arctangent function normalized in the range [0, 1] is assumed:

$$g(x) = \frac{1}{\pi}\arctan(\gamma x) + \frac{1}{2} \tag{33}$$

with $\gamma = 0.1$. The transfer function computes the signal output of a neuron from its signal inputs for both the hidden and the output layers; respectively, they are

$$H_j = g\left(\sum_{i=1}^{I} w_{ij} U_i\right) \quad 1 \le j \le J \tag{34}$$

$$S_k = g\left(\sum_{j=1}^{J+1} w_{jk} H_j\right) \quad 1 \le k \le K. \tag{35}$$

The parameters w_{ij} and w_{jk} are the so-called 'weighting factors' and constitute the free parameters to regress in the training process. In the present work a total of $J = 9$ neurons was chosen for the hidden layer, excluding the Bias2 term. There are consequently 27 weighting factors w_{ij} and 20 weighting factors w_{jk}, and there are then altogether 47 free parameters in the model. The number of neurons in the hidden layer was optimized by *trial-and-error*. The value $J = 9$ is set here as an ideal compromise between computation speed and flexibility of the resulting mathematical form for the representation of the considered fluids.

The output values S_k of the output layer neurons are de-normalized to real output variables W_k, which in this case are the shape functions θ_j and ϕ_j, through the following transformations:

$$W_k = \frac{S_k - A_{\min}}{s_k} + W_{k,\min} \qquad 1 \le k \le K \tag{36}$$

with

$$s_k = \frac{A_{\max} - A_{\min}}{W_{k,\max} - W_{k,\min}} \tag{37}$$

where

$$W_1 = \theta_j(T_j, \rho_j) \tag{38}$$

$$W_2 = \phi_j(T_j, \rho_j). \tag{39}$$

The values of $V_{i,\min}$ and $V_{i,\max}$ depend on the selected range of the variables for the studied fluid and are therefore fluid specific. For many of the considered fluids the values of $W_{\min}$ are set to 0.6 for both $\theta_{\min}$ and $\phi_{\min}$, while the values of $W_{\max}$ are set to 1.4 for both $\theta_{\max}$ and $\phi_{\max}$. Consequently, the shape functions are limited in the range [0.6, 1.4]. Anyway, for some fluids, a wider range, i.e., [0.4, 1.6], was chosen.

4.3. Calculation of Thermodynamic Properties

The availability of all the essential elements of the model, i.e., the basic EoS and the analytical forms of the shape functions, allows the derivation of any thermodynamic property function for the target fluid. As an example, the calculation of the two functions $u_j^{\mathrm{R}}(T_j, \rho_j)$ and $Z_j^{\mathrm{R}}(T_j, \rho_j)$, already mentioned in Eqs. (10) and (11), is demonstrated. From the cited equations the two functions read:

$$u_j^{\mathrm{R}} = u_0^{\mathrm{R}}(1 - F_T) - Z_0^{\mathrm{R}} H_T \tag{40}$$

$$Z_j^{\mathrm{R}} = u_0^{\mathrm{R}} F_\rho + Z_0^{\mathrm{R}}(1 + H_\rho). \tag{41}$$

In these equations the reduced residual functions indicated with the subscript 0 are obtained from the basic EoS, in the reduced residual Helmholtz energy form $a_0^{\mathrm{R}}(T_0, \rho_0)$, according to

$$Z_0^{\mathrm{R}} = \rho_0 \left(\frac{\partial a_0^{\mathrm{R}}}{\partial \rho_0} \right)_{T_0} \tag{42}$$

$$u_0^{\mathrm{R}} = \frac{U_0^{\mathrm{R}}}{R T_0} = -T_0 \left(\frac{\partial a_0^{\mathrm{R}}}{\partial T_0} \right)_{\rho_0}, \tag{43}$$

where the variables of the basic EoS are

$$T_0 = T_j / \theta_j \tag{44}$$

$$\rho_0 = \rho_j \phi_j. \tag{45}$$

In Eqs. (40) and (41) the derivatives of the shape functions F_T, H_T, F_ρ, and H_ρ are calculated from Eqs. (12)–(17). The shape functions and their derivatives are calculated at the present fluid conditions (T_j, ρ_j) following the neural network formalism presented in Section 4.2 and given in greater detail in the Appendix.

For the case when the assumed basic EoS is the SRK equation, Eq. (26), the analytical expressions for the a_0^R derivatives in Eqs. (42) and (43) read:

$$\left(\frac{\partial a_0^R}{\partial T_0}\right)_{\rho_0} = -\frac{1}{RT_0 b}\left(\frac{\partial a_{SRK}}{\partial T_0} - \frac{a_{SRK}}{T_0}\right)\ln\left[\frac{1+(c+b)\rho_0}{1+c\rho_0}\right] \tag{46}$$

$$\left(\frac{\partial a_0^R}{\partial \rho_0}\right)_{T_0} = -\frac{c-b}{1+(c-b)\rho_0} - \frac{a_{SRK}}{RT_0 b}\left[\frac{c+b}{1+(c+b)\rho_0} - \frac{c}{1+c\rho_0}\right], \tag{47}$$

where the derivative of the SRK coefficient a_{SRK} in Eq. (46) has to be calculated from Eq. (19). Any further thermodynamic property function can be obtained with analogous procedures using the mathematical expressions provided in the Appendix.

5. TRAINING OF THE EEOS–NN MODEL

5.1. Training Procedure

As previously explained, the present EEoS–NN modeling technique for pure fluids recovers all the formalism of the basic ECS method, with the basic EoS given by the SRK cubic equation, Eq. (26), and the two individual shape functions $\theta_j(T_j, \rho_j)$ and $\phi_j(T_j, \rho_j)$ represented through a MLFN. The coefficients of the shape functions in neural form are obtained for each fluid of interest with a regression procedure, indicated as *training*, using data of thermodynamic properties for the fluid itself. The training of the MLFN is performed minimizing an objective function, expressed in terms of mean squares, which can include properties of a different nature as in a multiproperty fitting framework [1–3].

In a first step of the present work the fluid-specific EEoS–NN model has been heuristically developed from volumetric and saturation properties assuming an objective function that includes two parts accounting for both contributions. The one for volumetric data reads

$$f_{ob,1} = \frac{1}{n_1}\sum_{i=1}^{n_1}\left[\frac{(Z_j^R)_i^{exp} - (Z_j^R)_i^{EEoS}}{(Z_j^R)_i^{exp}}\right]^2 \tag{48}$$

while that for saturation properties reads

$$f_{\mathrm{ob},2} = \frac{1}{n_2} \sum_{i=1}^{n_2} \left\{ \ln \varphi_j^{\mathrm{EEoS}}[T, \rho_{\mathrm{sl}}^{\mathrm{exp}}(T)] - \ln \varphi_j^{\mathrm{EEoS}}[T, \rho_{\mathrm{sv}}^{\mathrm{exp}}(T)] \right\}_i^2. \tag{49}$$

In these equations n_1 and n_2 are the numbers of points in the training sets for volumetric and saturation properties, respectively. Throughout this work the superscript "exp" indicates values generated from the DEoS of the target fluid and assumed as pseudo-experimental values, as explained in Section 5.2, while the subscripts "sl" and "sv" stand for saturated liquid and saturated vapor, respectively. It is recalled that the fugacity coefficient of a target fluid j in Eq. (49) is calculated as

$$\ln \varphi_j = g_j^{\mathrm{R}} - \ln(1 + Z_j^{\mathrm{R}}) \tag{50}$$

The two former objective functions, Eqs. (48) and (49), are combined together to form the overall objective function:

$$f_{\mathrm{ob,overall}} = \xi f_{\mathrm{ob},1} + (1 - \xi) f_{\mathrm{ob},2} \tag{51}$$

in which the functions $f_{\mathrm{ob},1}$ and $f_{\mathrm{ob},2}$ are differently weighted. The coefficient ξ was chosen from experience as an optimal value that balances the two contributions giving satisfactory results for both the properties; in the present case, it was set to the value 0.8.

In a second step of the study the EEoS–NN model has been regressed assuming an objective function which includes also caloric quantities, together with the unavoidable volumetric and saturation properties. The considered caloric properties are the isochoric heat capacity C_v, the isobaric heat capacity C_p, and the speed of sound w. The first part of the objective function $f_{\mathrm{ob},1}$ now reads

$$f_{\mathrm{ob},1} = \frac{1}{P n_1} \sum_{p=1}^{P} \xi_p \sum_{i=1}^{n_1} \left[\frac{(m_j)_i^{\mathrm{exp}} - (m_j)_i^{\mathrm{EEoS}}}{(m_j)_i^{\mathrm{exp}}} \right]_p^2. \tag{52}$$

In Eq. (52) the pth property m_j represents alternatively the residual compressibility factor Z^{R}, the residual isochoric heat capacity C_v^{R}, the residual isobaric heat capacity C_p^{R}, and the speed of sound w; thus, $P = 4$.

For each of the four properties the corresponding data set is composed of n_1 values and its contribution is weighted in the summation according to the individual factor ξ_p. The second component of the objective function $f_{\mathrm{ob},2}$ is represented by Eq. (49) again; the two parts are combined according to Eq. (51).

In both cases the training of the MLFN is performed through the minimization of Eq. (51) with conventional gradient descent techniques [31].

5.2. Generation of Values of Thermodynamic Properties

Since the main aims of the present work are to test the proposed modeling technique and to verify its performances for a group of pure fluids, it was decided to use generated data of thermodynamic properties instead of experimental data. In this way the results of the analysis are not affected by the drawbacks related to experimental data. In fact, these are in general affected by a significant experimental error noise, with a different accuracy for each thermodynamic quantity, and they are irregularly distributed in the (T, P) range of interest.

These aspects hinder the evaluation of the quality of a heuristic model. Thus, it was preferred not to use experimental values for the model training and validation, but rather to use pseudo-experimental values generated on a regular grid of the independent variables from the DEoSs of the studied fluids. The surfaces represented by these equations are considered as "true," as they are the best representation of the available experimental data base, and then the proposed method is evaluated in the most favorable conditions. The use of experimental data for obtaining a dedicated EoS for a pure fluid in the EEoS–NN format will be a matter of further work, once the technique has been consolidated.

Since the constraint of conformality between the target and the reference fluid affecting the ECS methods is in this work overcome, the considered fluids can belong to different chemical families. The chosen fluids, listed in Table I, are divided into a group of non-polar fluids (three alkanes), a group of polar fluids (four haloalkanes), and a group of strongly polar fluids (ammonia and water). The difficulties in accurately describing the properties of the selected fluids increase in this order.

Sets of values of several thermodynamic properties have been generated for each fluid from the corresponding DEoS in the temperature and pressure ranges indicated in Table II, taking care of having them distributed on a regular grid. The thermodynamic surface was divided into three regions: the liquid phase (denoted by "l") for $T < T_c$ and $P > P^{sat}$, the supercritical condition (denoted by "sc") for $T > T_c$ and $P > P_c$, and the vapor phase (denoted by "v") for the remaining domain.

Besides density and vapor–liquid equilibrium (VLE), the reduced residual functions of Helmholtz energy a^R, internal energy u^R, enthalpy h^R, Gibbs energy g^R, and entropy s^R were considered. These functions

Table II. Characteristics of the Pseudo-Experimental Data Generated from the DEoSs for the Considered Fluids

			Training NPT					Validation NPT				
			P, ρ, T					Each of nine properties[a]				
Fluid	T range (K)	P range (MPa)	sc	l	v	Overall	$P, \rho, T\|_{VLE}$	sc	l	v	Overall	$P, \rho, T\|_{VLE}$
C_2H_6	200–400	0.08–10	156	269	200	625	13	1174	2032	1498	4704	24
C_3H_8	200–400	0.08–10	56	462	107	625	21	406	3553	745	4704	40
n-C_4H_{10}	200–450	0.08–10	48	501	76	625	22	320	3856	528	4704	42
R32	200–400	0.08–10	67	396	162	625	18	492	3017	1195	4704	36
R125	200–400	0.08–10	128	380	117	625	17	906	2973	825	4704	33
R134a	200–400	0.08–10	60	476	89	625	21	380	3693	631	4704	41
R143a	200–400	0.08–10	112	401	112	625	18	808	3082	814	4704	34
NH_3	200–450	0.08–14	25	411	189	625	20	157	3151	1396	4704	39
H_2O	300–700	0.08–25	12	434	179	625	21	78	3335	1291	4704	41

[a] Properties: $Z^R, a^R, u^R, h^R, g^R, s^R, c_v^R, c_p^R, w$.

are indicated as "first-order" thermodynamic properties because they are analytically obtained by combining a^R and first-order derivatives of a^R.

Furthermore, thermodynamic properties involving higher-order derivatives of a^R, e.g., the reduced residual isochoric heat capacity c_v^R, the reduced residual isobaric heat capacity c_p^R, and the speed of sound w, were considered. These properties are called "second-order" properties.

For each fluid and for each property 5329 points were generated on the cited grid. From the generated data set, data subsets were extracted for the two training processes described in Section 5.1 and for the validation step. A similar procedure is followed for the VLE data.

For the first training process the distribution of the training and validation data sets can be seen in Table II. The subset used for training was obtained regularly extracting density values from the generated data on the original grid. For the validation set the remaining values of the density grid were used together with points for the other properties.

For the second training step, the data for each of the four thermodynamic quantities included in the objective function, Eq. (52), were regularly extracted from the same original grid as well, but with a larger interval. The validation set is again composed of the remaining values. The number of points used in the second training step is reported in Table III.

Table III. Dimensions of the Training and Validation Sets for the Considered Fluids in the Multiproperty Case

	Training NPT					Validation NPT				
	Each of four properties[a]					Each of nine properties[b]				
Fluid	sc	l	v	Overall	$P, \rho, T\|_{VLE}$	sc	l	v	Overall	$P, \rho, T\|_{VLE}$
C_2H_6	28	52	37	117	13	1302	2249	1661	5212	24
C_3H_8	14	80	23	117	21	448	3935	829	5212	40
n-C_4H_{10}	8	92	17	117	22	360	4265	587	5212	42
R32	13	73	31	117	18	546	3340	1326	5212	36
R125	24	69	24	117	17	1010	3284	918	5212	33
R134a	16	83	18	117	21	424	4086	702	5212	41
R143a	24	70	23	117	18	896	3413	903	5212	34
NH_3	6	75	36	117	20	176	3487	1549	5212	39
H_2O	4	115	50	169	21	86	3654	1420	5160	41

[a] Properties: Z^R, c_v^R, c_p^R, w.

[b] Properties: $Z^R, a^R, u^R, h^R, g^R, s^R, c_v^R, c_p^R, w$.

6. VALIDATION PROCEDURES

During the training procedure described in Section 5.1 an equation in the EEoS–NN format was obtained for each considered fluid by regression of the data in its training set. In the present section, the performances of these models and of the cubic equation assumed as a reference are evaluated with respect to the data of the validation sets; see Section 5.2.

Throughout this work the deviations of the data from the model are expressed in terms of the average absolute deviation (AAD), which is defined as

$$\mathrm{AAD}(\%) = \frac{100}{\mathrm{NPT}} \sum_{i=1}^{\mathrm{NPT}} \left| \frac{m^{\mathrm{exp}} - m^{\mathrm{mod}}}{m^{\mathrm{exp}}} \right|_i \tag{53}$$

for the generic property m, where the superscript "mod" stands for the value calculated from the model to be validated and NPT denotes the number of points of the data set.

6.1. Accuracy of a Cubic EoS: Case of SRK with Volume Translation

The predictions of the SRK cubic EoS with respect to first- and second-order thermodynamic properties were tested for the nine fluids listed in Table I. The results for the first-order properties are presented in detail for each fluid in Table IV. The following conclusions can be drawn from these results:

- notwithstanding the Peneloux volume translation, the prediction accuracy of the SRK equation for density is still far from being comparable to that of a DEoS, particularly for polar fluids. This can be argued looking at the results for Z^{R} in particular for R32, R143a, ammonia, and water. Even for simple alkanes, the prediction accuracy is not homogeneous for different regions of the $P\rho T$ surface;
- increased errors are observed for properties involving the a^{R} derivative with respect to temperature, such as u^{R}, h^{R}, and s^{R}. For them it was verified that the deviations are sometimes higher than 20% in the vapor region of the $P\rho T$ surface;
- for polar fluids the accuracy is usually worse than for non-polar ones; in fact, the alkanes are described better than the other substances.

The second-order properties are considered in Table V, where the heat capacities are examined both as residual and as overall quantities. Deviations for these properties are larger than for properties involving only first derivatives. For some fluids the AADs for the residual heat capacities are very high and in particular for c_v^{R} they increase to average values above

Table IV. Accuracy of the SRK Equation in Terms of AAD for First-Order Properties in the Three Main Thermodynamic Regions

	AAD (%)								
	Z^R			u^R			h^R		
Fluid	sc	l	v	sc	l	v	sc	l	v
C_2H_6	3.79	0.75	1.37	3.44	1.44	5.44	2.59	1.32	4.05
C_3H_8	4.68	0.73	1.72	3.05	1.18	6.87	3.35	1.10	5.12
n-C_4H_{10}	4.83	0.77	2.27	3.59	1.26	9.53	3.77	1.18	6.97
R32	5.99	0.77	7.06	7.87	2.83	19.67	7.44	2.59	16.30
R125	5.76	0.81	2.83	3.81	1.07	11.38	3.04	0.98	7.84
R134a	5.67	0.77	3.28	4.95	1.41	14.38	5.03	1.32	11.34
R143a	6.70	0.91	4.86	3.31	1.99	12.14	3.88	1.84	10.09
NH_3	3.51	0.54	5.49	9.60	2.85	21.16	8.13	2.60	16.95
H_2O	2.24	0.70	6.76	11.67	4.51	19.16	9.24	4.17	14.22
Mean	**5.16**	**0.75**	**4.23**	**4.39**	**2.06**	**13.94**	**4.04**	**1.90**	**10.86**
	a^R			g^R			s^R		
Fluid	sc	l	v	sc	l	v	sc	l	v
C_2H_6	3.24	1.83	1.73	3.47	1.49	1.49	4.96	2.53	9.31
C_3H_8	6.23	1.44	1.85	5.66	1.21	1.73	1.78	2.13	12.04
n-C_4H_{10}	6.60	1.37	2.45	5.96	1.17	2.29	2.44	2.17	16.87
R32	9.05	2.91	7.58	7.87	2.33	7.33	7.02	5.31	27.07
R125	7.11	1.64	3.42	6.58	1.37	3.14	8.25	2.15	21.25
R134a	8.17	1.79	3.09	7.26	1.49	3.17	3.32	2.46	21.44
R143a	8.80	2.28	5.10	8.03	1.88	4.99	2.70	4.01	17.04
NH_3	4.40	2.40	5.32	4.08	1.92	5.39	12.93	5.02	30.78
H_2O	5.67	3.12	8.03	3.84	2.59	7.29	18.96	31.19	7.29
Mean	**6.50**	**2.07**	**4.60**	**5.99**	**1.71**	**4.38**	**5.34**	**6.44**	**18.10**

40%. The error is obviously reduced when the ideal part is considered as well. Nonetheless, it is clear that the SRK EoS is not at all effective for the residual part of this group of properties. The accuracy of calculated speeds of sound in the liquid and supercritical regions ranges from 5 to 25% for all the fluids, while the accuracy in the vapor phase is significantly better. The results are very similar for non-polar and polar fluids.

Results for the representation of saturation properties are reported in Table V. The saturation densities are predicted with rather high deviations and with an evident difference between the liquid and vapor phases. For the saturated liquid the deviations for all the fluids amount to several per cent units showing that, notwithstanding the density correction at the temperature of $T_r = 0.7$ due to the volume translation, the basic trend of

Table V. Accuracy of the SRK Equation in Terms of AAD for Second-Order Properties in the Three Main Thermodynamic Regions and for Saturation Properties

AAD (%)									
	c_v^R			c_p^R			w		
Fluid	sc	l	v	sc	l	v	sc	l	v
C_2H_6	34.44	57.36	53.95	7.20	13.99	13.66	5.21	22.13	0.41
C_3H_8	30.22	63.19	70.30	10.16	8.01	25.82	7.88	23.44	0.36
n-C_4H_{10}	26.94	65.74	72.73	11.23	8.12	30.20	9.65	22.83	0.39
R32	52.17	28.11	75.42	16.04	19.28	16.04	12.75	22.36	1.73
R125	34.35	58.55	68.05	10.13	7.56	23.78	7.17	26.34	0.73
R134a	27.30	40.07	74.44	13.00	10.22	36.84	8.87	24.38	0.55
R143a	36.07	50.77	71.26	11.87	11.64	32.01	8.31	25.15	0.91
NH_3	70.46	12.07	80.49	18.85	19.22	45.05	16.18	14.43	2.34
H_2O	76.14	22.18	81.53	25.64	33.69	48.56	20.18	13.45	2.29
Mean	**36.99**	**44.26**	**71.78**	**11.17**	**14.48**	**30.18**	**8.34**	**21.61**	**1.24**
	C_v			C_p			Saturation properties		
Fluid	sc	l	v	sc	l	v	P^{sat}	ρ_{sl}	ρ_{sv}
C_2H_6	3.85	9.66	2.81	4.17	6.80	2.42	0.88	5.31	0.55
C_3H_8	3.16	8.72	3.15	5.54	3.26	3.53	1.01	4.59	0.92
n-C_4H_{10}	2.34	7.63	2.48	5.00	2.66	3.18	1.49	4.09	1.41
R32	14.33	9.96	10.32	11.30	11.04	10.28	1.83	6.86	3.41
R125	4.31	9.33	3.66	5.08	3.25	3.27	0.85	5.12	0.80
R134a	4.58	8.16	4.99	7.46	4.49	5.85	1.22	4.91	1.51
R143a	5.32	9.30	4.42	6.31	5.04	4.85	1.38	5.69	1.83
NH_3	25.64	5.30	14.74	13.79	11.37	13.62	2.35	6.00	4.33
H_2O	36.23	12.58	18.81	20.18	19.81	17.02	5.37	8.67	5.47
Mean	**6.44**	**8.90**	**8.39**	**6.48**	**7.41**	**8.02**	**1.90**	**5.71**	**2.35**

a cubic EoS for the dense phase is substantially wrong. The behavior for the saturated vapor density is far better, but this is probably due to the modest contribution of the residual density function in the vapor region, where the ideal part prevails.

The vapor pressure P^{sat} is rather well represented without a relevant systematic error. This behavior is coherent with the specialization of cubic EoSs in representing this property, since the function $\alpha(T_r)$, Eqs. (21) and (22), was regressed by Soave [19] on vapor-pressure data for several fluids.

In summary, it can be concluded that the representation of thermodynamic properties by the SRK cubic EoS is not satisfying, in particular, when second-order properties are considered.

6.2. Validation of the EEoS–NN Models Trained on Density and Coexistence Data

In a first step the EEoS–NN model was trained for each of the fluids listed in Table I solely on volumetric and saturation data, following the regression procedure presented in Section 5.1. Nine fluid-specific EoSs in this format were obtained. The coefficients of the equations for ethane, R32, and ammonia are given in Table VI as examples for the reader's convenience.

The training procedure yields the MLFN equations for the shape functions $\theta_j(T_j, \rho_j)$ and $\phi_j(T_j, \rho_j)$ of the target fluid. In Figs. 2 and 3 the two functions are plotted for R32 as an example, showing a quite regular trend for both of them. The method is very effective in reproducing the shape of the thermodynamic surface with limited distortions of the independent variables.

The performance of the obtained EEoS–NN models is evaluated in terms of overall deviation d_{overall}, which is a linear combination of the volumetric deviation d_1 and of the vapor–liquid coexistence condition d_2:

$$d_1 = \frac{1}{n_1} \sum_{i=1}^{n_1} \left| \frac{(Z_j^{\text{R}})_i^{\text{exp}} - (Z_j^{\text{R}})_i^{\text{EEoS}}}{(Z_j^{\text{R}})_i^{\text{exp}}} \right| \tag{54}$$

$$d_2 = \frac{1}{n_2} \sum_{i=1}^{n_2} \left| \ln \varphi_j^{\text{EEoS}}[T, \rho_{\text{sl}}^{\text{exp}}(T)] - \ln \varphi_{\text{j}}^{\text{EEoS}}[T, \rho_{\text{sv}}^{\text{exp}}(T)] \right|_i \tag{55}$$

$$d_{\text{overall}} = 0.8 d_1 + 0.2 d_2 \tag{56}$$

The weights of the two components of the overall deviation, i.e., 0.8 for the volumetric deviation and 0.2 for the coexistence condition, are the same as those assumed for the definition of the objective function, Eq. (51).

The results of the training process are reported in Table VII. The overall deviations found for the training and the validation data sets are very close each others and the validation values are never greater than the training ones. This is an indirect proof that overfitting was avoided in the regressions. For both quantities the deviations are very low, showing that the proposed modeling technique is effective in representing a thermodynamic surface for which a discrete set of local values is given as input.

The deviations of the EEoS–NN models with respect to the data of the validation sets are summarized in Table VIII for first-order properties, separately for the three main thermodynamic regions. The representation of these quantities can be considered excellent for all properties, and the deviations are quite similar for all fluids without any noteworthy decrease of accuracy.

Table VI. Parameters of the EEoS–NN Equations for Some of the Considered Fluids

C_2H_6						R32					
I	3		Bias1	1.00		I	3		Bias1	1.00	
J	9		Bias2	1.00		J	9		Bias2	1.00	
K	2		A_{min}	0.05		K	2		A_{min}	0.05	
γ	0.1		A_{max}	0.95		γ	0.1		A_{max}	0.95	
$V_{1,min} \equiv T_{min}$	200 K		$V_{1,max} \equiv T_{max}$	400 K		$V_{1,min} \equiv T_{min}$	200 K		$V_{1,max} \equiv T_{max}$	400 K	
$V_{2,min} \equiv \rho_{min}$	$0.0711\ mol \cdot L^{-1}$		$V_{2,max} \equiv \rho_{max}$	$17.7878\ mol \cdot L^{-1}$		$V_{2,min} \equiv \rho_{min}$	$0.0236\ mol \cdot L^{-1}$		$V_{2,max} \equiv \rho_{max}$	$24.6785\ mol \cdot L^{-1}$	
$W_{1,min} \equiv \theta_{min}$	0.4		$W_{1,max} \equiv \theta_{max}$	1.6		$W_{1,min} \equiv \theta_{min}$	0.6		$W_{1,max} \equiv \theta_{max}$	1.4	
$W_{2,min} \equiv \phi_{min}$	0.4		$W_{2,max} \equiv \phi_{max}$	1.6		$W_{2,min} \equiv \phi_{min}$	0.6		$W_{2,max} \equiv \phi_{max}$	1.4	
i	j	w_{ij}	i	j	w_{ij}	i	j	w_{ij}	i	j	w_{ij}
1	1	−14.6800	1	9	−19.7707	1	1	25.8062	1	9	−0.980788
2	1	−36.7225	2	9	17.9822	2	1	7.87380	2	9	28.3954
3	1	−0.524619	3	9	−0.921700	3	1	0.206814	3	9	−12.3360
1	2	−7.98044	j	k	w_{jk}	1	2	1.48621	j	k	w_{jk}
2	2	36.6931	1	1	34.3968	2	2	13.9058	1	1	7.43770
3	2	−17.0923	2	1	9.83861	3	2	−13.8027	2	1	−5.51264
1	3	−17.0805	3	1	2.47472	1	3	7.48193	3	1	17.1968
2	3	−34.1314	4	1	−18.3624	2	3	29.3472	4	1	−34.1528
3	3	29.1315	5	1	−16.3998	3	3	−20.1814	5	1	23.2390
1	4	−4.26496	6	1	−17.9008	1	4	65.8419	6	1	−22.2816
2	4	8.74906	7	1	17.3222	2	4	44.3238	7	1	−26.7759
3	4	−11.4438	8	1	17.5252	3	4	−2.67600	8	1	12.4071
1	5	15.7066	9	1	−11.1595	1	5	−22.9148	9	1	−13.6838
2	5	5.88812	10	1	8.22283	2	5	−2.99058	10	1	38.3822
3	5	−16.3387	1	2	−24.8961	3	5	37.3539	1	2	18.0280
1	6	−3.46601	2	2	−30.6647	1	6	22.9680	2	2	17.4574

2	6	14.4387	3	2	−24.0579	2	6	43.1282	3	2	19.6204
3	6	−0.598933	4	2	7.63339	3	6	−12.8855	4	2	−33.7625
1	7	−22.0176	5	2	7.44584	1	7	−11.1055	5	2	−15.3131
2	7	−16.4412	6	2	19.0711	2	7	18.8999	6	2	−21.6972
3	7	2.23637	7	2	10.4056	3	7	2.42737	7	2	33.2710
1	8	6.60631	8	2	−21.7495	1	8	−12.6540	8	2	30.3163
2	8	12.0352	9	2	33.2215	2	8	23.3375	9	2	−34.1808
3	8	−5.27018	10	2	−1.76478	3	8	1.33904	10	2	1.57788

NH_3				R32 (multiproperty case)			
I	3	Bias1	1.00	I	3	Bias1	1.00
J	9	Bias2	1.00	J	9	Bias2	1.00
K	2	$A_{\min}$	0.05	K	2	$A_{\min}$	0.05
γ	0.1	$A_{\max}$	0.95	γ	0.1	$A_{\max}$	0.95
$V_{1,\min} \equiv T_{\min}$	200 K	$V_{1,\max} \equiv T_{\max}$	450 K	$V_{1,\min} \equiv T_{\min}$	200 K	$V_{1,\max} \equiv T_{\max}$	400 K
$V_{2,\min} \equiv \rho_{\min}$	$0.0211\,\mathrm{mol \cdot L^{-1}}$	$V_{2,\max} \equiv \rho_{\max}$	$43.0175\,\mathrm{mol \cdot L^{-1}}$	$V_{2,\min} \equiv \rho_{\min}$	$0.0236\,\mathrm{mol \cdot L^{-1}}$	$V_{2,\max} \equiv \rho_{\max}$	$24.6785\,\mathrm{mol \cdot L^{-1}}$
$W_{1,\min} \equiv \theta_{\min}$	0.4	$W_{1,\max} \equiv \theta_{\max}$	1.6	$W_{1,\min} \equiv \theta_{\min}$	0.6	$W_{1,\max} \equiv \theta_{\max}$	1.4
$W_{2,\min} \equiv \phi_{\min}$	0.4	$W_{2,\max} \equiv \phi_{\max}$	1.6	$W_{2,\min} \equiv \phi_{\min}$	0.6	$W_{2,\max} \equiv \phi_{\max}$	1.4

i	j	w_{ij}	i	j	w_{ij}	i	j	w_{ij}	i	j	w_{ij}
1	1	−0.0343471	1	9	2.41861	1	1	32.3217	1	9	−0.715001
2	1	38.9817	2	9	5.82662	2	1	16.5637	2	9	19.6418
3	1	−1.30222	3	9	−18.5690	3	1	−3.42176	3	9	−10.0246
1	2	4.75296	j	k	w_{jk}	1	2	−2.07609	j	k	w_{jk}
2	2	18.4242	1	1	−29.6304	2	2	232771	1	1	12.2450
3	2	−14.6645	2	1	16.2682	3	2	−18.0462	2	1	−3.64476
1	3	−47.5350	3	1	16.9999	1	3	6.41524	3	1	16.3958
2	3	−59.0826	4	1	8.99122	2	3	26.9161	4	1	−37.9539

Table VI. (*Continued*)

3	3	1.15102	5	1	−3.21625	3	3	−19.2222	5	1	22.9462
1	4	2.57659	6	1	−0.563209	1	4	79.0332	6	1	−22.1000
2	4	58.2927	7	1	29.2292	2	4	48.7375	7	1	−26.3712
3	4	1.54064	8	1	12.9465	3	4	−4.51428	8	1	13.7960
1	5	11.8164	9	1	−10.9797	1	5	−18.6620	9	1	−13.6306
2	5	17.7896	10	1	0.243259	2	5	−9.72398	10	1	36.7859
3	5	8.58851	1	2	40.2369	3	5	35.2427	1	2	20.9745
1	6	−5.26532	2	2	11.7392	1	6	20.9904	2	2	19.4342
2	6	21.4480	3	2	37.1241	2	6	45.5368	3	2	20.8848
3	6	−21.7151	4	2	61.6914	3	6	−13.9584	4	2	−34.7121
1	7	−21.0200	5	2	−21.9731	1	7	−13.5759	5	2	−15.8031
2	7	−78.3444	6	2	−18.0815	2	7	23.3505	6	2	−31.7282
3	7	13.7091	7	2	26.3947	3	7	3.27104	7	2	31.6253
1	8	22.0313	8	2	−28.5963	1	8	−17.1427	8	2	29.5093
2	8	23.2789	9	2	10.6949	2	8	25.8225	9	2	−35.9755
3	8	2.37419	10	2	−52.4756	3	8	6.30393	10	2	2.93842

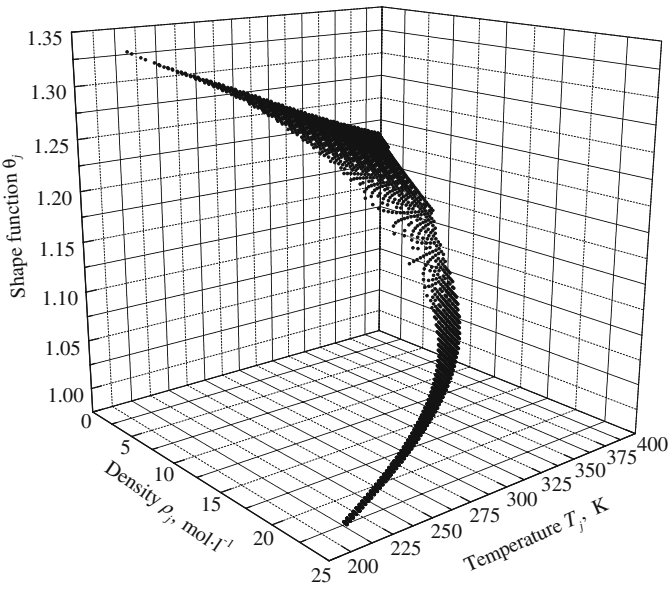

Fig. 2. Shape function $\theta_j = \theta(Tj, \rho_j)$ for the target fluid R32.

The three thermodynamic regions are represented with small differences; while the liquid phase is always described with an excellent accuracy, for the vapor phase some fluctuations of accuracy were found but without an apparent regularity in the dependence on the fluid. In the supercritical region the model behaves quite similarly as in the vapor. Properties involving the temperature derivative of a^{R} are represented with a lower accuracy. This can be explained by the fact that the model was not trained on quantities involving temperature derivatives; except for the coexistence curve, only a volumetric property was given as input and this one solely involves the density derivative of a^{R}, see Eq. (11).

The EEoS–NN models were also checked for the accuracy in predicting the second-order properties; the results are presented in Table IX. Both residual heat capacities are represented with an accuracy which is worse by one or two orders of magnitude with respect to those of the first-order properties. Moreover, deviations for the residual isochoric heat capacity are roughly three times worse than deviations for the residual isobaric heat capacity.

Fortunately these thermodynamic properties are used in practice only as overall quantities. For the overall heat capacities the deviations are significantly reduced and become comparable with current experimental uncertainties. This is evidently due to a "dilution" of the error in the

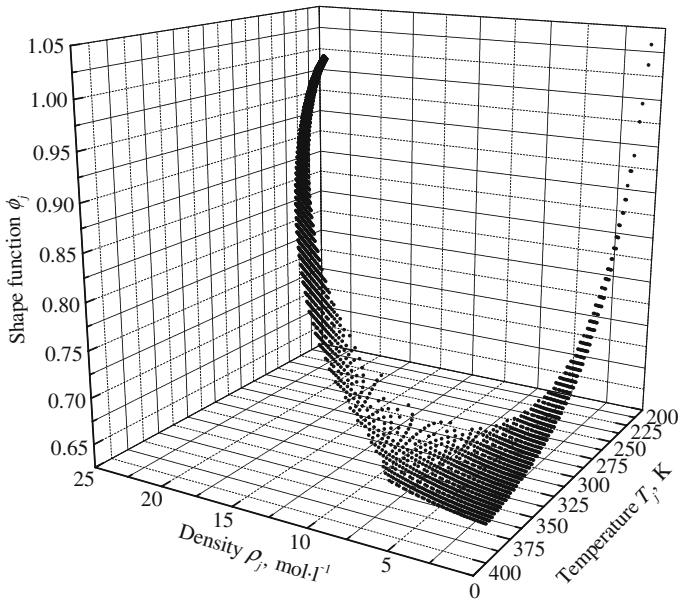

Fig. 3. Shape function $\phi_j = \phi(Tj, \rho_j)$ for the target fluid R32.

summation of ideal and residual parts. In general, deviations increase from the vapor to the liquid and to the supercritical region. The overall heat capacity functions in the vapor phase are often represented very well, whereas for the other regions their precision can be considered acceptable. The speed of sound is well represented in the vapor phase, but for the other regions the performance is worse, although it is anyway comparable with that of a multiparameter DEoS.

The comparison for saturation densities and vapor pressures, reported in Table IX, shows satisfactory performance, in particular, for the liquid density and the vapor pressure. As a conclusion the proposed model can produce quite reliable results also for the prediction of those thermodynamic quantities involving higher-order derivatives of a^R, notwithstanding that no input was given for them during the training procedure. In fact the EEoS–NN model trained only on density and coexistence data can satisfactorily predict second-order properties.

6.3. Validation of the EEoS–NN Models Trained on Multiproperty Data

A procedure similar to that formerly discussed at Section 6.2 was performed for the models trained on values of the four thermodynamic

Table VII. Comparison between the Values of the Deviation Function Obtained for Training and Validation Sets

Fluid	Training $d_{overall}$	Validation $d_{overall}$
C_2H_6	0.185×10^{-3}	0.185×10^{-3}
C_3H_8	0.296×10^{-3}	0.278×10^{-3}
n-C_4H_{10}	0.221×10^{-3}	0.211×10^{-3}
R32	0.175×10^{-3}	0.174×10^{-3}
R125	0.358×10^{-3}	0.334×10^{-3}
R134a	0.154×10^{-3}	0.151×10^{-3}
R143a	0.178×10^{-3}	0.167×10^{-3}
NH_3	0.338×10^{-3}	0.336×10^{-3}
H_2O	0.442×10^{-3}	0.415×10^{-3}

Table VIII. Accuracy of the EEoS–NN Models in Terms of AAD for First-Order Properties in the Three Main Thermodynamic Regions

	AAD (%)								
	Z^R			u^R			h^R		
Fluid	sc	l	v	sc	l	v	sc	l	v
C_2H_6	0.030	0.001	0.040	0.118	0.078	0.250	0.094	0.067	0.181
C_3H_8	0.100	0.001	0.089	0.258	0.072	0.265	0.219	0.063	0.199
n-C_4H_{10}	0.048	0.001	0.056	0.387	0.052	0.320	0.316	0.046	0.234
R32	0.045	0.001	0.047	0.169	0.063	0.242	0.137	0.055	0.184
R125	0.056	0.002	0.119	0.302	0.051	0.917	0.240	0.045	0.644
R134a	0.047	0.001	0.058	0.222	0.039	0.279	0.187	0.036	0.216
R143a	0.031	0.001	0.031	0.279	0.059	0.277	0.218	0.053	0.204
NH_3	0.137	0.002	0.085	0.331	0.069	0.528	0.279	0.061	0.403
H_2O	0.271	0.002	0.065	0.392	0.050	0.275	0.347	0.045	0.216
Mean	**0.053**	**0.001**	**0.064**	**0.236**	**0.058**	**0.368**	**0.191**	**0.051**	**0.273**
	a^R			g^R			s^R		
Fluid	sc	l	v	sc	l	v	sc	l	v
C_2H_6	0.030	0.018	0.034	0.030	0.013	0.035	0.191	0.151	0.447
C_3H_8	0.119	0.016	0.094	0.112	0.012	0.091	0.377	0.132	0.426
n-C_4H_{10}	0.083	0.011	0.042	0.068	0.009	0.047	0.605	0.095	0.542
R32	0.058	0.017	0.034	0.053	0.014	0.038	0.261	0.116	0.381
R125	0.080	0.011	0.170	0.065	0.008	0.130	0.484	0.089	1.716
R134a	0.073	0.012	0.036	0.062	0.009	0.044	0.315	0.071	0.435
R143a	0.043	0.018	0.029	0.037	0.014	0.029	0.459	0.106	0.460
NH_3	0.186	0.016	0.063	0.167	0.012	0.070	0.448	0.132	0.836
H_2O	0.385	0.013	0.056	0.339	0.010	0.057	0.443	0.094	0.405
Mean	**0.070**	**0.014**	**0.059**	**0.062**	**0.011**	**0.058**	**0.367**	**0.107**	**0.614**

Table IX. Accuracy of the EEoS–NN Models in Terms of AAD for Second-Order Properties in the Three Main Thermodynamic Regions and for Saturation Properties

AAD (%)									
	c_v^R			c_p^R			w		
Fluid	sc	l	v	sc	l	v	sc	l	v
C_2H_6	5.004	8.860	6.285	0.663	1.888	1.665	0.335	0.410	0.029
C_3H_8	13.436	5.797	2.392	2.200	1.384	1.090	0.872	0.352	0.061
n-C_4H_{10}	16.540	3.921	4.900	2.764	0.959	1.383	0.535	0.189	0.037
R32	7.286	3.453	4.601	1.360	1.236	1.805	0.832	0.305	0.095
R125	10.200	3.827	7.442	1.565	0.800	2.903	0.487	0.383	0.026
R134a	8.568	2.809	4.788	1.875	1.003	2.063	0.728	0.176	0.030
R143a	9.398	6.037	4.637	1.392	1.864	1.432	0.401	0.279	0.030
NH_3	7.360	2.851	6.411	3.569	1.375	2.739	0.734	0.566	0.182
H_2O	3.208	1.665	1.864	4.558	1.300	1.128	1.123	0.935	0.057
Mean	**8.834**	**4.149**	**4.883**	**1.567**	**1.278**	**1.831**	**0.545**	**0.393**	**0.069**
	C_v			C_p			Saturation properties		
Fluid	sc	l	v	sc	l	v	P^{sat}	ρ_{sl}	ρ_{sv}
C_2H_6	0.569	1.555	0.297	0.367	0.850	0.304	0.061	0.010	0.073
C_3H_8	1.199	0.801	0.137	1.333	0.532	0.343	0.066	0.089	0.211
n-C_4H_{10}	1.250	0.425	0.233	1.312	0.306	0.259	0.068	0.047	0.165
R32	1.871	1.206	0.612	0.928	0.679	0.499	0.064	0.064	0.172
R125	1.160	0.590	0.346	0.800	0.328	0.347	0.059	0.102	0.206
R134a	1.304	0r.651	0.401	1.132	0.439	0.492	0.050	0.009	0.069
R143a	1.298	1.220	0.250	0.741	0.783	0.209	0.066	0.015	0.068
NH_3	2.650	1.227	1.173	2.857	0.789	0.964	0.073	0.025	0.137
H_2O	1.817	0.962	0.393	4.275	0.746	0.432	0.047	0.048	0.153
Mean	**1.192**	**0.916**	**0.481**	**0.929**	**0.587**	**0.461**	**0.061**	**0.046**	**0.142**

quantities Z^R, c_v^R, c_p^R, w plus the ones on the coexistence curve. As an example, the coefficients of the equation obtained in this case for R32 are given in Table VI.

Comparing the results for the training on density and coexistence data, which were presented in Table VIII, with the results of the multiproperty training reported in Table X, it can be seen that the prediction of first-order properties becomes globally worse for more or less all the properties, but in general the difference is not significant.

For the second-order properties, Table XI shows that there is an evident improvement of performance for the isochoric heat capacity in all the regions and for the isobaric heat capacity in the liquid phase, both as residual and as overall values. For some fluids this improvement is larger,

Table X. Accuracy of the EEoS–NN Models in the Multiproperty Case in Terms of AAD for First-Order Properties in the Three Main Thermodynamic Regions

AAD (%)									
	Z^R			u^R			h^R		
Fluid	sc	l	v	sc	l	v	sc	l	v
C_2H_6	0.063	0.003	0.063	0.111	0.016	0.226	0.095	0.014	0.163
C_3H_8	0.128	0.002	0.164	0.220	0.039	0.384	0.197	0.034	0.312
n-C_4H_{10}	0.092	0.002	0.122	0.190	0.010	0.334	0.166	0.009	0.250
R32	0.197	0.002	0.112	0.325	0.041	0.519	0.287	0.036	0.379
R125	0.094	0.002	0.283	0.091	0.031	0.459	0.088	0.027	0.255
R134a	0.102	0.002	0.136	0.242	0.016	0.410	0.196	0.014	0.314
R143a	0.136	0.002	0.232	0.159	0.049	0.889	0.148	0.044	0.637
NH_3	0.615	0.009	0.417	0.905	0.036	1.162	0.731	0.033	0.910
H_2O	0.744	0.002	0.095	1.267	0.098	0.323	1.142	0.088	0.255
Mean	**0.136**	**0.003**	**0.183**	**0.208**	**0.037**	**0.541**	**0.183**	**0.033**	**0.402**
	a^R			g^R			s^R		
Fluid	sc	l	v	sc	l	v	sc	l	v
C_2H_6	0.076	0.006	0.061	0.069	0.005	0.060	0.154	0.027	0.420
C_3H_8	0.147	0.024	0.123	0.139	0.019	0.137	0.293	0.060	0.647
n-C_4H_{10}	0.150	0.021	0.092	0.124	0.016	0.102	0.227	0.017	0.542
R32	0.199	0.013	0.121	0.201	0.011	0.109	0.459	0.065	0.853
R125	0.095	0.014	0.451	0.080	0.010	0.343	0.121	0.058	1.176
R134a	0.132	0.006	0.110	0.120	0.005	0.119	0.348	0.027	0.632
R143a	0.117	0.027	0.227	0.123	0.022	0.227	0.221	0.066	1.466
NH_3	0.719	0.037	0.391	0.673	0.030	0.395	1.193	0.043	1.691
H_2O	1.099	0.028	0.077	0.953	0.021	0.082	1.411	0.197	0.477
Mean	**0.153**	**0.020**	**0.185**	**0.143**	**0.016**	**0.177**	**0.279**	**0.063**	**0.892**

especially for the isochoric heat capacity. The performance for the speed of sound remains at the same level as before with some small variations depending on the specific fluid.

The comparisons for the coexistence locus, reported in Table XI, are also very promising. The obtained accuracy is similar to the accuracy resulting from the training to first-order properties, see Table IX.

The inclusion of data for second-order quantities into the training set improves the EEoS–NN model for such properties, obtaining a more satisfactory performance for them. In fact, in this case information about higher-order derivatives of a^R is supplied to the model.

Table XI. Accuracy of the EEoS–NN Models in the Multiproperty Case in Terms of AAD for Second-Order Properties in the Three Main Thermodynamic Regions and for Saturation Properties

AAD (%)									
	c_v^R			c_p^R			w		
Fluid	sc	l	v	sc	l	v	sc	l	v
C_2H_6	2.695	1.367	3.464	0.832	0.355	1.227	0.288	0.194	0.019
C_3H_8	1.929	1.292	1.399	2.154	0.318	1.042	0.323	0.408	0.046
n-C_4H_{10}	1.989	0.711	1.768	1.760	0.170	0.927	0.581	0.184	0.038
R32	2.778	0.706	2.710	2.250	0.388	1.162	0.931	0.291	0.059
R125	3.493	0.469	2.615	0.626	0.173	1.040	0.262	0.180	0.047
R134a	3.672	0.870	3.045	1.496	0.185	1.692	0.445	0.290	0.100
R143a	1.822	0.948	2.469	0.713	0.123	1.061	0.302	0.256	0.051
NH_3	5.725	0.939	3.258	6.613	0.363	1.652	1.713	0.617	0.197
H_2O	3.750	1.329	1.862	6.658	1.214	1.289	1.532	0.666	0.076
Mean	**2.792**	**0.946**	**2.628**	**1.493**	**0.363**	**1.261**	**0.456**	**0.348**	**0.075**
	C_v			C_p			Saturation properties		
Fluid	sc	l	v	sc	l	v	P^{sat}	ρ_{sl}	ρ_{sv}
C_2H_6	0.387	0.224	0.250	0.554	0.182	0.307	0.011	0.038	0.224
C_3H_8	0.211	0.187	0.082	1.478	0.130	0.320	0.085	0.065	0.192
n-C_4H_{10}	0.174	0.077	0.071	1.203	0.059	0.163	0.098	0.061	0.209
R32	0.856	0.243	0.477	1.767	0.229	0.406	0.041	0.075	0.151
R125	0.418	0.073	0.107	0.312	0.078	0.141	0.019	0.053	0.103
R134a	0.635	0.171	0.319	1.045	0.086	0.452	0.061	0.044	0.141
R143a	0.272	0.174	0.195	0.428	0.055	0.227	0.087	0.016	0.158
NH_3	2.221	0.399	0.709	5.613	0.213	0.727	0.140	0.136	0.596
H_2O	2.055	0.752	0.396	6.092	0.712	0.530	0.191	0.110	0.344
Mean	**0.501**	**0.254**	**0.335**	**1.036**	**0.192**	**0.398**	**0.087**	**0.069**	**0.240**

7. CHOOSING THE NUMBER OF POINTS OF THE TRAINING SET: CASE OF ETHANE

The discussed modeling technique is able to heuristically develop a pure-fluid fundamental DEoS based on a limited number of data. The question is now posed about how much it is possible to reduce the number of points composing the training set without compromising the final result, i.e., how limited the experimental effort necessary for the development of a DEoS in this format can be. Using generated data as before, tests on how many data points are required to guarantee a good performance of the EEoS–NN model were made. The fluid ethane was chosen for the analysis.

In this particular study reference is made to the training case in which only density and coexistence data are used as input for the regression; the details of the training process are described in Section 5.1. At that point more than 600 P, ρ, T data points were included into the training set together with a very limited number of coexistence data. Starting from the original number of 625 points, six training cases, in which the number of density points in the training set is reduced by 50% each time, are now considered. The obtained models are validated with respect to the values of the remaining points of the original grid composed of 5329 points, see Table II.

The values of the objective function $f_{\text{ob,overall}}$ and of the deviation d_{overall} obtained for each case are plotted in Fig. 4 for both the training and the validation data as functions of the number of points in the training set. As this number gets smaller, the $f_{\text{ob,overall}}$ and d_{overall} functions for the training set improve. At the same time the accuracy of predictions decreases, particularly when the number of points becomes smaller than 100. Cases 5 and 6 represent extreme conditions since for them the number of input data for the regression is lower than the number of parameters to determine; in these circumstances, the regression produces an unacceptable overfitting. Anyway, with more than 100 P, ρ, T points for training, the prediction accuracy of the model is satisfying and overfitting is avoided.

8. CONCLUSIONS

The traditional ECS approach for the representation of thermodynamic properties of pure fluids has been revised in conjunction with one of the most effective general function approximator techniques, i.e., the neural networks. In previous studies the basic requirements of the ECS theory were maintained, searching for the conformality between reference and target fluids. In the present work a step forward is taken developing an innovative EEoS–NN method using a basic EoS for the fluid of interest. Such an EoS can be generic as for instance a cubic equation, which can be set up for practically any fluid because it requires only the critical data and a few vapor-pressure values to get the acentric factor.

This eliminates the need for choosing a reference fluid conformal with the target fluid and for the availability of a DEoS to represent the reference fluid with the highest accuracy. The new method can be used to develop a fundamental DEoS for any target fluid, where suitable experimental data in the range of interest are available. The technique is not restricted to the choice of a cubic EoS but any fundamental EoS in the independent variables T, ρ, on which the shape functions distortion has to

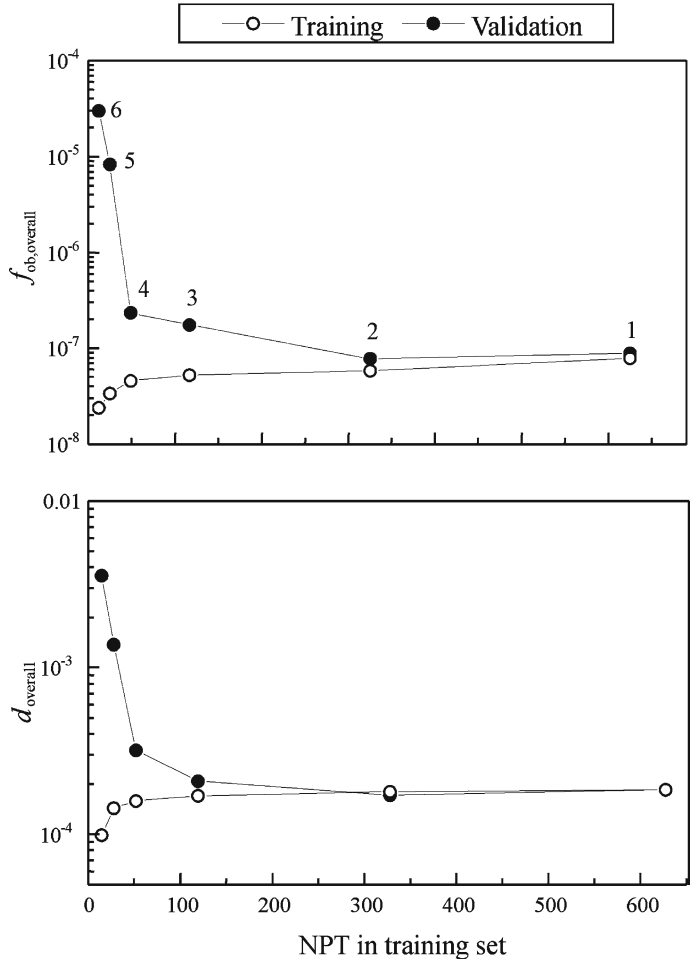

Fig. 4. Objective $f_{ob,overall}$ and deviation $d_{overall}$ functions and their dependence on the number of points in the training set: case of ethane.

be applied, can be suitably considered, independently from the functional form of the EoS.

The EEoS–NN modeling technique has been extensively tested for a sample of nine pure fluids including non-polar, polar, and strongly polar substances. For the studied fluids pseudo-experimental thermodynamic data, generated from substance-specific DEoSs, have been used in order to avoid disturbances due to scatter and uneven distribution of the

available experimental data. The model requires a few hundred P, ρ, T data points distributed on the thermodynamic surface inside the region of interest and a small number of coexistence data as input. As a result, it can represent any thermodynamic property, including "second-order" thermodynamic properties like isochoric and isobaric heat capacities and speed of sound. If data for second-order properties are added to the training set, the accuracy of the EEoS–NN model for these properties increases.

The use of a neural network as a function approximator in such a model compensates for the initially low accuracy of the basic EoS. The EEoS–NN method is a promising and innovative modeling technique for the heuristic development of a DEoS for a pure fluid from multiproperty data, and it is an alternative to the presently available most advanced heuristic methods.

APPENDIX

Calculation of Thermodynamic Properties for a Pure Fluid from an Equation of State in the EEoS–NN Format

The equations required for the calculation of the thermodynamic properties of a pure fluid according to the proposed EEoS–NN format are given here. As previously explained, the subscript j refers to the fluid of interest, while the subscript 0 denotes values calculated from the basic equation for the model, which in the present case is the SRK cubic EoS with Peneloux volume translation [18, 19, 22]. The independent variables of the EEoS model and of the basic equation are related by

$$T_0 = T_j/\theta_j \qquad \rho_0 = \rho_j \phi_j \tag{A1,A2}$$

The main thermodynamic properties considered in this work are obtained as follows:

$$\text{Compressibility factor:} \quad Z_j^{\mathrm{R}} \equiv P_j/\rho_j RT_j - 1 = F_\rho u_0^{\mathrm{R}} + (1 + H_\rho) Z_0^{\mathrm{R}} \tag{A3}$$

$$\text{Helmholtz energy:} \quad a_j^{\mathrm{R}} = A_j^{\mathrm{R}}/RT_j = a_0^{\mathrm{R}} \tag{A4}$$

$$\text{Internal energy:} \quad u_j^{\mathrm{R}} = U_j^{\mathrm{R}}/RT_j = (1 - F_T) u_0^{\mathrm{R}} - H_T Z_0^{\mathrm{R}} \tag{A5}$$

$$\text{Enthalpy:} \quad h_j^{\mathrm{R}} = H_j^{\mathrm{R}}/RT_j = h_0^{\mathrm{R}} + (F_\rho - F_T) u_0^{\mathrm{R}} + (H_\rho - H_T) Z_0^{\mathrm{R}} \tag{A6}$$

$$\text{Gibbs energy:} \quad g_j^{\mathrm{R}} = G_j^{\mathrm{R}}/RT_j = g_0^{\mathrm{R}} + F_\rho u_0^{\mathrm{R}} + H_\rho Z_0^{\mathrm{R}} \tag{A7}$$

$$\text{Entropy:} \quad s_j^{\mathrm{R}} = S_j^{\mathrm{R}}/R = s_0^{\mathrm{R}} - F_T u_0^{\mathrm{R}} - H_T Z_0^{\mathrm{R}} \tag{A8}$$

$$\text{Isochoric heat capacity:} \quad c_{v,j}^{\mathrm{R}} = C_{v,j}^{\mathrm{R}}/R = -T_j^2 \left(\frac{\partial^2 a_j^{\mathrm{R}}}{\partial T_j^2} \right)_{\rho_j} + 2u_j^{\mathrm{R}} \tag{A9}$$

$$\text{Isobaric heat capacity:} \quad c_{p,j}^{\mathrm{R}} = C_{p,j}^{\mathrm{R}}/R = c_{v,j}^{\mathrm{R}} + \frac{\left[1 + Z_j^{\mathrm{R}} + \rho_j T_j \left(\frac{\partial^2 a_j^{\mathrm{R}}}{\partial \rho_j \partial T_j} \right) \right]^2}{1 + 2Z_j^{\mathrm{R}} + \rho_j^2 \left(\frac{\partial^2 a_j^{\mathrm{R}}}{\partial \rho_j^2} \right)_{T_j}} - 1 \tag{A10}$$

$$\text{Speed of sound:} \quad w_j = \sqrt{\frac{RT_j}{M_j} \frac{C_{p,j}}{C_{v,j}} \left[1 + 2Z_j^{\mathrm{R}} + \rho_j^2 \left(\frac{\partial^2 a_j^{\mathrm{R}}}{\partial \rho_j^2} \right)_{T_j} \right]} \tag{A11}$$

$$\begin{aligned} \text{Fugacity coefficient:} \quad \ln \varphi_j &= g_j^{\mathrm{R}} - \ln(1 + Z_j^{\mathrm{R}}) \\ &= a_j^{\mathrm{R}} + Z_j^{\mathrm{R}} - \ln(1 + Z_j^{\mathrm{R}}) \end{aligned} \tag{A12}$$

The second derivatives in Eqs. (A9)–(A11) are calculated with the following equations:

$$\begin{aligned} T_j^2 \left(\frac{\partial^2 a_j^{\mathrm{R}}}{\partial T_j^2} \right)_{\rho_j} &= T_0^2 \left(\frac{\partial^2 a_0^{\mathrm{R}}}{\partial T_0^2} \right)_{\rho_0} (1 - F_T)^2 + 2\rho_0 T_0 \left(\frac{\partial^2 a_0^{\mathrm{R}}}{\partial \rho_0 \partial T_0} \right) H_T (1 - F_T) \\ &\quad + Z_0^{\mathrm{R}} H_{TT} - u_0^{\mathrm{R}} (2F_T^2 - 2F_T - F_{TT}) + \rho_0^2 \left(\frac{\partial^2 a_0^{\mathrm{R}}}{\partial \rho_0^2} \right)_{T_0} H_T^2 \end{aligned} \tag{A13}$$

$$\begin{aligned} \rho_j^2 \left(\frac{\partial^2 a_j^{\mathrm{R}}}{\partial \rho_j^2} \right)_{T_j} &= T_0^2 \left(\frac{\partial^2 a_0^{\mathrm{R}}}{\partial T_0^2} \right)_{\rho_0} F_\rho^2 - 2\rho_0 T_0 \left(\frac{\partial^2 a_0^{\mathrm{R}}}{\partial \rho_0 \partial T_0} \right) F_\rho (1 + H_\rho) \\ &\quad + Z_0^{\mathrm{R}} (2H_\rho + H_{\rho\rho}) - u_0^{\mathrm{R}} (2F_\rho^2 - F_{\rho\rho}) + \rho_0^2 \left(\frac{\partial^2 a_0^{\mathrm{R}}}{\partial \rho_0^2} \right)_{T_0} (1 + H_\rho)^2 \end{aligned} \tag{A14}$$

$$\begin{aligned}\rho_j T_j \left(\frac{\partial^2 a_j^{\mathrm{R}}}{\partial \rho_j \partial T_j}\right) = {} & T_0^2 \left(\frac{\partial^2 a_0^{\mathrm{R}}}{\partial T_0^2}\right)_{\rho_0} F_\rho (F_T - 1) \\ & + \rho_0 T_0 \left(\frac{\partial^2 a_0^{\mathrm{R}}}{\partial \rho_0 \partial T_0}\right) [(1 + H_\rho)(1 - F_T) - F_\rho H_T] \\ & + Z_0^{\mathrm{R}} (H_T + H_{\rho T}) - u_0^{\mathrm{R}} (2 F_T F_\rho - F_\rho - F_{\rho T}) \\ & + \rho_0^2 \left(\frac{\partial^2 a_0^{\mathrm{R}}}{\partial \rho_0^2}\right)_{T_0} H_T (1 + H_\rho)\end{aligned} \tag{A15}$$

The logarithmic derivatives of the shape functions are defined as

$$F_\rho \equiv \frac{\rho_j}{\theta_j}\left(\frac{\partial \theta_j}{\partial \rho_j}\right)_{T_j} \qquad H_\rho \equiv \frac{\rho_j}{\phi_j}\left(\frac{\partial \phi_j}{\partial \rho_j}\right)_{T_j} \tag{A16, A17}$$

$$F_T \equiv \frac{T_j}{\theta_j}\left(\frac{\partial \theta_j}{\partial T_j}\right)_{\rho_j} \qquad H_T \equiv \frac{T_j}{\phi_j}\left(\frac{\partial \phi_j}{\partial T_j}\right)_{\rho_j} \tag{A18, A19}$$

$$F_{\rho\rho} \equiv \frac{\rho_j^2}{\theta_j}\left(\frac{\partial^2 \theta_j}{\partial \rho_j^2}\right)_{T_j} \qquad H_{\rho\rho} \equiv \frac{\rho_j^2}{\phi_j}\left(\frac{\partial^2 \phi_j}{\partial \rho_j^2}\right)_{T_j} \tag{A20, A21}$$

$$F_{TT} \equiv \frac{T_j^2}{\theta_j}\left(\frac{\partial^2 \theta_j}{\partial T_j^2}\right)_{\rho_j} \qquad H_{TT} \equiv \frac{T_j^2}{\phi_j}\left(\frac{\partial^2 \phi_j}{\partial T_j^2}\right)_{\rho_j} \tag{A22, A23}$$

$$F_{\rho T} \equiv \frac{\rho_j T_j}{\theta_j}\left(\frac{\partial^2 \theta_j}{\partial \rho_j \partial T_j}\right) \qquad H_{\rho T} \equiv \frac{\rho_j T_j}{\phi_j}\left(\frac{\partial^2 \phi_j}{\partial \rho_j \partial T_j}\right) \tag{A24, A25}$$

If the SRK cubic equation is selected as the basic equation for the EEoS model, the quantities in Eqs. (A3)–(A15) are calculated with the following expressions:

$$a_0^{\mathrm{R}} = -\ln[1 + (c - b)\rho_0] - \frac{a_{\mathrm{SRK}}}{R T_0 b} \ln\left[\frac{1 + (c + b)\rho_0}{1 + c\rho_0}\right] \tag{A26}$$

$$Z_0^{\mathrm{R}} = -\frac{(c - b)\rho_0}{1 + (c - b)\rho_0} - \frac{a_{\mathrm{SRK}}}{R T_0 b}\left[\frac{(c + b)\rho_0}{1 + (c + b)\rho_0} - \frac{c\rho_0}{1 + c\rho_0}\right] \tag{A27}$$

$$u_0^{\mathrm{R}} = \frac{1}{Rb}\left(\frac{\partial a_{\mathrm{SRK}}}{\partial T_0} - \frac{a_{\mathrm{SRK}}}{T_0}\right) \ln\left[\frac{1 + (c + b)\rho_0}{1 + c\rho_0}\right] \tag{A28}$$

$$h_0^{\mathrm{R}} = u_0^{\mathrm{R}} + Z_0^{\mathrm{R}} \tag{A29}$$

$$g_0^{\mathrm{R}} = a_0^{\mathrm{R}} + Z_0^{\mathrm{R}} \tag{A30}$$

$$s_0^{\mathrm{R}} = u_0^{\mathrm{R}} - a_0^{\mathrm{R}} \tag{A31}$$

$$\left(\frac{\partial^2 a_0^{\mathrm{R}}}{\partial T_0^2}\right)_{\rho_0} = -\frac{1}{RbT_0}\left(\frac{\partial^2 a_{\mathrm{SRK}}}{\partial T_0^2} - \frac{2}{T_0}\frac{\partial a_{\mathrm{SRK}}}{\partial T_0} + \frac{2a_{\mathrm{SRK}}}{T_0^2}\right)\ln\left[\frac{1+(c+b)\rho_0}{1+c\rho_0}\right] \tag{A32}$$

$$\left(\frac{\partial^2 a_0^{\mathrm{R}}}{\partial \rho_0^2}\right)_{T_0} = \left[\frac{(c-b)}{1+(c-b)\rho_0}\right]^2 + \frac{a_{\mathrm{SRK}}}{RT_0 b}\left\{\left[\frac{(c+b)}{1+(c+b)\rho_0}\right]^2 - \left(\frac{c}{1+c\rho_0}\right)^2\right\} \tag{A33}$$

$$\left(\frac{\partial^2 a_0^{\mathrm{R}}}{\partial \rho_0 \partial T_0}\right) = -\frac{1}{RbT_0}\left(\frac{\partial a_{\mathrm{SRK}}}{\partial T_0} - \frac{a_{\mathrm{SRK}}}{T_0}\right)\left[\frac{(c+b)}{1+(c+b)\rho_0} - \frac{c}{1+c\rho_0}\right] \tag{A34}$$

In the present work the shape functions are obtained in the form of a multi-layer feedforward neural network. The equations for the calculation of the shape functions and their derivatives are reported in the following. The correspondence of the physical variables of the system with the variables of the neural model is given by

$$V_1 = T_j \qquad V_2 = \rho_j \tag{A35, A36}$$

$$W_1 = \theta_j \qquad W_2 = \phi_j \tag{A37, A38}$$

Neural network inputs

$$U_i = u_i(V_i - V_{i,\min}) + A_{\min} \quad \text{with} \quad u_i = \frac{A_{\max} - A_{\min}}{V_{i,\max} - V_{i,\min}} \quad \text{for} \quad 1 \le i \le I-1 \tag{A39, A40}$$

$$U_I = \mathrm{Bias1} \tag{A41}$$

Hidden layer inputs and outputs

$$G_j = \sum_{i=1}^{I} w_{ij} U_i \qquad 1 \le j \le J \tag{A42}$$

$$H_j = g\left(\sum_{i=1}^{I} w_{ij} U_i\right) \qquad 1 \le j \le J \tag{A43}$$

$$H_{J+1} = \mathrm{Bias2} \tag{A44}$$

Output layer inputs and outputs

$$R_k = \sum_{j=1}^{J+1} w_{jk} H_j \qquad 1 \le k \le K \tag{A45}$$

$$S_k = g(R_k) \qquad 1 \le k \le K \tag{A46}$$

Physical variable outputs

$$W_k = \frac{S_k - A_{\min}}{s_k} + W_{k,\min} \quad \text{with} \quad s_k = \frac{A_{\max} - A_{\min}}{W_{k,\max} - W_{k,\min}} \quad \text{for} \quad 1 \le k \le K \tag{A47, A48}$$

Output derivatives

$$\frac{\partial W_k}{\partial V_m} = \frac{u_m}{s_k} g'(R_k) \sum_{j=1}^{J} w_{mj} w_{jk} g'(G_j) \qquad 1 \le m \le I-1, 1 \le k \le K \tag{A49}$$

$$\frac{\partial^2 W_k}{\partial V_m \partial V_n} = \frac{u_m u_n}{s_k} g''(R_k) \left[\sum_{j=1}^{J} w_{mj} w_{jk} g'(G_j) \right] \left[\sum_{j=1}^{J} w_{nj} w_{jk} g'(G_j) \right] + g'(R_k) \left[\sum_{j=1}^{J} w_{mj} w_{nj} w_{jk} g''(G_j) \right] \qquad 1 \le m, n \le I-1, 1 \le k \le K \tag{A50}$$

where

$$g(x) = \frac{1}{\pi} \arctan(\gamma x) + \frac{1}{2} \tag{A51}$$

$$g'(x) = \frac{\mathrm{d}g(x)}{\mathrm{d}x} = \frac{\gamma}{\pi[1 + (\gamma x)^2]} \tag{A52}$$

$$g''(x) = \frac{\mathrm{d}^2 g(x)}{\mathrm{d}x^2} = \frac{-2\gamma^3 x}{\pi[1 + (\gamma x)^2]^2} \tag{A53}$$

REFERENCES

1. R. Schmidt and W. Wagner, *Fluid Phase Equilib.* **19**:175 (1985).
2. U. Setzmann and W. Wagner, *Int. J. Thermophys*. **10**:1103 (1989)
3. R. Span, *Multiparameter Equations of State* (Springer Verlag, Berlin, 2000).
4. J. F. Ely, *Adv. Cryog. Eng*. **35**:1511 (1990).
5. M. Huber and J. F. Ely, *Int. J. Refrig*. **17**:18 (1994).
6. J. F. Estela-Uribe and J. P. M. Trusler, *Fluid Phase Equilib.* **150-151**:225 (1998).
7. J. F. Estela-Uribe and J. P. M. Trusler, *Fluid Phase Equilib.* **183-184**:21 (2001).
8. J. F. Estela-Uribe and J. P. M. Trusler, *Fluid Phase Equilib.* **204**:15 (2003).
9. J. F. Estela-Uribe and J. P. M. Trusler, *Fluid Phase Equilib.* **216**:59 (2004).
10. G. Scalabrin, L. Piazza, and G. Cristofoli, *Int. J. Thermophys*. **23**:57 (2002).
11. L. Piazza, G. Scalabrin, P. Marchi, and D. Richon, *Int. J. Refrig*. **29**:1182 (2006).
12. G. Scalabrin, L. Piazza, and D. Richon, *Fluid Phase Equilib.* **199**:33 (2002).
13. T. M. Reed and K. E. Gubbins, *Applied Statistical Mechanics* (McGraw-Hill, New York, 1973).
14. J. S. Rowlinson and F. L. Swinton, *Liquids and Liquid Mixtures* (Butterworths, London, 1982).
15. J. S. Rowlinson and I. D. Watson, *Chem. Eng. Sci*. **24**:1565 (1969).
16. T. W. Leland and P. S. Chappelear, *Ind. Eng. Chem*. **60**:15 (1968).
17. G. Scalabrin, P. Marchi, L. Bettio, and D. Richon, *Int. J. Refrig*. **29**:1195 (2006).
18. O. Redlich and J. N. S. Kwong, *Chem. Rev*. **44**:233 (1949).
19. G. Soave, *Chem. Eng. Sci*. **27**:1197 (1972).
20. J. Mollerup, *Fluid Phase Equilib.* **4**:11 (1980).
21. R. C. Reid, J. M. Prausnitz, and B. E. Poling, *The Properties of Gases and Liquids* (McGraw-Hill, New York, 1988).
22. A. Peneloux, E. Rauzy, and R. Freze, *Fluid Phase Equilib.* **8**:7 (1982).
23. D. G. Friend, H. Ingham, and J. F. Ely, *J. Phys. Chem. Ref. Data* **20**:275 (1991).
24. B. A. Younglove and J. F. Ely, *J. Phys. Chem. Ref. Data* **16**:577 (1987).
25. R. Tillner-Roth and A. Yokozeki, *J. Phys. Chem. Ref. Data* **26**:1273 (1997).
26. S. L. Outcalt and M. O. McLinden, *Int. J. Thermophys*. **16**:79 (1995).
27. R. Tillner-Roth and H. D. Baehr, *J. Phys. Chem. Ref. Data* **23**:657 (1994).
28. S. L. Outcalt and M. O. McLinden, *Int. J. Thermophys*. **18**:1445 (1997).
29. R. Tillner-Roth, F. Harms-Watzenberg, and H. D. Baehr, *Proc. 20th DKV-Tagungsbericht*, Vol. II (Heidelberg, Germany, 1993), pp. 167-181.
30. W. Wagner and A. Pruss, *J. Phys. Chem. Ref. Data* **31**:387 (2002).
31. D. E. Rumelhart and J. L. McClelland, *Parallel Distributed Processing: Exploration in the Microstructure of Cognition* (MIT Press, Cambridge, MA, 1986).